Simulation of water isotopes in combustion-derived vapor emissions in winter

Yan Yang[1] and Kei Yoshimura[2]

[1]Graduate School of Frontier Sciences, The University of Tokyo

[2]Institute of Industrial Science, The University of Tokyo

Key points

- The emission of combustion-derived vapor (CDV) was simulated with the isotopic-enable regional spectral model.
- The CDV addition reduced the water vapor d-excess and made the simulation align better with the observations in Salt Lake City.
- The CDV inclusion significantly increased the vapor d-excess variability with varying wind directions.

Abstract

With urbanization, anthropogenic water vapor emissions have become a significant component of the urban atmosphere. Fossil fuel combustion-derived vapor (CDV) is a primary source of these emissions. Owing to the notably low CDV d-excess, stable hydrogen and oxygen isotopes are promising for distinguishing CDV from natural sources. Considering the limitations of in situ observations, this study aims to explore the feasibility of using IsoRSM, an isotopically enabled regional atmospheric model, to simulate CDV emissions in urban areas in winter. Two experiments were conducted: one in Salt Lake City in January 2017 and another in Beijing in January 2007. The simulation results showed that the CDV addition significantly reduced the water vapor d-excess, particularly when the boundary layer was stable. The simulation with CDV emissions aligned better with the time series of in situ observations in Salt Lake City. The modification led to a more pronounced positive correlation between vapor d-excess and specific humidity, which was similar to the observation of Salt Lake City. The CDV inclusion significantly increased the vapor d-excess variability with varying wind directions in both sites. However, in Beijing, the underestimation of d-excess variation from natural sources caused a bigger discrepancy between the observed and simulated d-excess and CDV fraction. Thus, though there were still biases, the inclusion of CDV could improve the accuracy of isotopic simulation in the urban regions where CDV was one of the controlling factors of vapor d-excess.

Plain Language Summary

Combustion-derived vapor (CDV) generated from fossil fuel is one of the main sources of the anthropogenic water emission in urban areas. Water d-excess, which is calculated with the water isotopes of oxygen ($\delta^{18}O$) and hydrogen ($\delta^{2}H$), is usually be used to distinguish the water from different sources. Due to the extreme low d-excess of CDV, we can use the water isotopes to partition CDV from naturally evaporating water. Different from previous researched on CDV based on the in-situ observed data, this study aims to simulate the isotopic composition of CDV in urban areas with the atmospheric model. The results of experiments in Salt Lake City and Beijing indicates that CDV can be the one of the controlling factors of the vapor d-excess in some urban regions, and the inclusion of CDV in the model will improve the accuracy of simulation in these regions. Therefore, this approach has great potential for making the simulation of water isotopes on a global scale with the impact of the anthropogenic emissions.

1 Introduction

The impact of anthropogenic emissions on the hydrological cycle in urban areas has become increasingly significant with urbanization (Moriwaki et al., 2008; Tie et al., 2017; Ueyama et al., 2021). In winter, the specific humidity in the boundary layer over cities is often approximately 10% higher than that over the surrounding rural areas (Salmon et al., 2017). This phenomenon can be attributed to various factors, including vapor emissions from anthropogenic sources (Li et al., 2021). One major contributor to anthropogenic water vapor emissions is the combustion of fossil fuels. According to the annual carbon emissions and the emission ratio of CO_2 to H_2O (Gorski et al., 2015), fossil fuel combustion releases approximately 21.1 Pg/a of water into the atmosphere. Although this combustion-derived vapor (CDV) is negligible at the global and annual scales in the hydrologic cycle (Huntington, 2006; Loaiciga A' et al., 1996), it plays a significant role in urban hydrologic cycling and meteorology because of the concentrated spatial and temporal distributions of fossil fuel emissions (Bergeron & Strachan, 2012; Sailor, 2011).

CDV can affect the urban air quality and meteorology; it can also directly affect the radiative balance by increasing the water vapor concentrations, influencing the aerosol and cloud properties, and modifying the local or downwind precipitation (Carlton & Turpin, 2013; Fiorella et al., 2018; McCarthy et al., 2010; Rosenfeld et al., 2008). Previous studies have demonstrated that CDV contributes on average an additional 4.6 μg m^{-3} of PM2.5 during severely polluted conditions in the Guanzhong Basin, China. This additional CDV-induced PM2.5 corresponds on average to 5.1% of the local anthropogenic PM2.5 (Xing et al., 2020). The observation in Beijing also revealed that the CDV increases with aggravation of haze (Wu et al., 2022). Temporal variations of the fraction of CDV showed an obvious correlation with the intensity of human activities (Liu et al., 2022).

Conducting standard meteorological measurements is difficult to isolate the anthropogenic vapor from natural sources. However, during inversion periods in winter, there is a notable negative correlation between vapor d-excess ($d = \delta^2H - 8 \times \delta^{18}O$) and atmospheric CO_2 concentration (Gorski et al., 2015). Laboratory combustion experiments have demonstrated that the CDV d-excess ranges from -470‰ to -180‰, thereby being significantly lower than that of other natural sources (Blossey et al., 2010; Dansgaard, 1964; Fiorella et al., 2015). Due to this distinct difference, stable water vapor isotopes offer a promising approach for differentiating between observed water vapor originating from combustion and advection sources.

In 2008, the Isotope-Enabled Global Spectral Model (IsoGSM) was introduced as a three-dimensional stable water isotope model that operates at the global scale and covers multiple decades of data (Kei Yoshimura & Kanamitsu, 2008). This model considers both kinetic and equilibrium fractionation processes to determine the isotopic ratios in vapor, while the complex atmospheric processes are considered by incorporating a spectral nudging technique. A regional version of IsoGSM called Isotope-Enabled Regional Spectral Model (IsoRSM) was also developed, offering higher temporal and spatial resolutions (Kei Yoshimura et al., 2010); however, water emitted from fossil fuel combustion is not explicitly considered in this model. Therefore, the influence of anthropogenic vapor emissions on the model results has not been verified or validated, with the model focusing primarily on natural processes and not considering the impact of human-induced emissions on stable water

isotopes.

Most current studies on CDV focus on in situ measurements and observations; however, conducting continuous in situ observations over a long-time scale often involves various limitations (Wei et al., 2019). To propose a new approach to study on the impact of CDV and make further analysis on CDV and other meteorological factors, this study aimed to develop a CDV emission model within the IsoRSM and investigate whether incorporating CDV emissions improved the accuracy of isotopic simulations. The results were compared with in situ observational data to assess the performance of the model. Furthermore, the fractionation of CDV in the atmosphere was calculated to examine whether the boundary layer conditions affected the CDV dispersion.

2 Methodology

2.1 Model simulation

Yoshimura et al. (2010) introduced the IsoRSM, which is an enhanced version of the regional spectral model of the Scripps Experimental Climate Prediction Center (Kanamitsu et al., 2005). The IsoRSM incorporates the isotopic species of water vapor as tracers. In this model, no isotopic fractionation occurs during dynamic advection, ice and snow sublimation, terrestrial evapotranspiration (where 100% transpiration is assumed), and runoff processes. However, thermodynamic equilibrium fractionation occurs during most phase transitions—such as condensation and evaporation—among the gaseous, liquid, and solid phases of water under saturated conditions (Majoube, 1971a,b.). In addition, kinetic fractionation is considered for evaporation and isotopic exchange between open water and liquid raindrops with ambient air under unsaturated conditions, as well as condensation from vapor to ice at temperatures below -20 ℃ under supersaturated conditions (Xiaoyang Li et al., 2021; Merlivat & Jouzel, 1979).

The IsoRSM utilizes a spectral nudging technique to enhance the simulation of atmospheric circulation and improve the realism of the model (Kanamaru & Kanamitsu, 2007). This technique involves forcing large-scale temperature and wind fields in the model towards the reanalysis forcing fields. Thus, the model captures broader atmospheric circulation patterns and their interactions with the global climate system. On the contrary, small-scale details, which are influenced by local geographic features, such as topography, land–sea distribution, and land use, are considered in the IsoRSM. This allows the model to maintain the local characteristics and capture the interplay between atmospheric circulation and the specific geographic features of the region, thereby contributing to a more accurate representation of the regional climate (Kanamitsu et al., 2010; Kie Yoshimura & Kanamitsu, 2009).

To address the Gibbs phenomenon, the Non-iteration Dimensional-Split Semi-Lagrangian (NDSL) advection scheme was implemented in IsoRSM. The Gibbs phenomenon arises when positive-definite quantities, such as moisture and tracers, generate negative values owing to the spectral space transformation employed in spectral model systems. To overcome this issue, the spectral prognostic specific humidity and radioactive tracer advection schemes in the IsoRSM were replaced with the NDSL advection scheme. Unlike spectral space transformations, the NDSL scheme considers the advection of tracers within a grid system

without spectral calculations. By employing the NDSL scheme, negative specific humidity values produced during spectral calculations can be eliminated without sacrificing the detailed features and accuracy of the model. This helps to alleviate the Gibbs phenomenon and ensures more reliable simulations using the IsoRSM (Chang & Yoshimura, 2015).

2.2 Observational data

Observational isotopic data from Salt Lake City (SLC) were collected by (Fiorella et al., 2019) between December 2016 and February 2017. To maintain data continuity, only data from January 2017 were used in this experiment. The isotopic ratio of vapor in SLC was measured using a Picarro L2130-i analyzer.Observational isotopic data for Beijing were obtained from the Stable Water Vapor Isotopes Database (SWVID) and covered the period from December 2006 to December 2007 (Wen et al., 2010). The isotopic ratio of vapor in Beijing was measured using a Campbell TGA-100A Trace Gas Analyzer.Meteorological data of these two sites, such as 2-m air temperature and 2-m specific humidity, were obtained from the ERA5 reanalysis dataset (Hersbach et al., 2020).

2.3 Experiment design

In this study, an additional quantity of vapor characterized by a fixed isotopic ratio was introduced into the evaporation process of the IsoRSM to simulate the CDV emissions. To simulate the urban area, CDV was added within a 2°×2° domain, whereas the rest of the domain represented natural sources without CDV emissions. This allowed to focus specifically on the CDV impact on the urban environment while maintaining a comparison with natural sources in the surrounding area.

Two experiments were conducted, one in SLC, USA (40.77° N, 111.85° W), and one in Beijing, China (40.00° N, 116.38° E). **Table 1** presents an overview of the key experimental details. SLC is situated in Salt Lake Valley and is characterized by a basin topography on a plateau. Previous studies have indicated that during winter, the boundary layer in this region can become highly stable due to temperature inversions, resulting in the formation of "persistent cold air pools" (PCAPs). During this period, elevated levels of CO_2, vapor, and pollutants are evident, leading to significantly lower d-excess values. Conversely, Beijing is located in the North China Plain, which is significantly influenced by the summer and winter monsoons. These two sites are relatively close in latitude, allowing for a comparative analysis of how the CDV impact is influenced by these distinct topographies and climates. Considering the greater CDV influence in winter and the limitations of the observation period, the experiments in SLC and Beijing were conducted in January 2017 and January 2007, respectively.

The isotopic composition of the added vapor was determined based on laboratory combustion experiments conducted in Xi'an, China (Xing et al., 2020). Specifically, the δ^2H and $\delta^{18}O$ values of the added vapor were set to -134.4‰ and 9‰, respectively. To estimate the order of magnitude of the CDV emission rate to be added, the annual CO_2 emission rate in urban areas and the emission ratio of CO_2 to CDV were considered (Hirano et al., 2015; Mckain et al., 2012; Moriwaki et al., 2008; Pisso et al., 2019). In this experiment, the CDV emission rates were set to six different values, from 0.000 to 0.003 $g/m^2 \cdot s$, to check which

rate exhibited the highest correlation with the observations. The selected emission rate after validation would be used in the subsequent analysis.

Table 1 Information and data sources of two experiments

	SLC	Beijing
Starting & ending time	2017/1/1 – 2017/1/31	2007/1/1 – 2007/1/31
Domain area	39 - 41°N 111 -113°W	39 - 41°N 115 -117°E
Topography	Basin	Plain
Climate type	Continental	Monsoon
Output time step	1 hour	
Boundary condition of simulation	IsoGSM	
Observed isotopic data source	(Fiorella *et al*., 2019)	SWVID (Wen *et al*., 2010)
Meteorological data source for validation	ERA5 reanalysis dataset	

2.4 CDV fraction

The CDV fraction in the total moisture is also an important variable for studying the CDV impact on the urban atmosphere. In this study, two different methods were used to calculate the CDV fraction. The first approach was the moisture tracer approach. In the IsoRSM, it is possible to tag the moisture in a certain domain or amount and trace its diffusion and transportation. This approach is typically used to analyze the moisture sources of a domain or event. Using this method, the CDV that was added to the model was tagged, so that the specific humidity caused by the CDV could be simulated and the CDV fraction could be directly calculated by the proportion of the CDV amount and the total humidity.

The second approach involved the use of a two-end-member mixing equation to calculate the CDV fraction in the atmosphere. By comparing the simulation results before and after the modification, it was possible to estimate the CDV contribution to atmospheric humidity. The moistening of the lower troposphere by CDV can be modeled as a mixing process between the CDV and background natural water vapor. The equation for this mixing process is as follows:

$$d_{\mathrm{mix}} = \frac{d_{\mathrm{CDV}} q_{\mathrm{CDV}} + d_{\mathrm{nat}} q_{\mathrm{nat}}}{q_{\mathrm{mix}}}.$$

Here, the subscripts CDV, nat, and mix represent the properties of the CDV, atmospheric moisture in the absence of CDV, and the values of the mixed parcel, respectively. In this study, the mixed parcel can be considered as the result after the CDV addition, whereas the

atmospheric moisture without CDV can be regarded as the result before the modification. q_{mix} represents the total specific humidity in the mixed parcel. Using the constraint that $q_{\mathrm{mix}} = q_{\mathrm{CDV}} + q_{\mathrm{nat}}$, the CDV fraction can be calculated as follows:

$$\frac{q_{\mathrm{CDV}}}{q_{\mathrm{mix}}} = \frac{d_{\mathrm{mix}} - d_{\mathrm{nat}}}{d_{\mathrm{CDV}} - d_{\mathrm{nat}}}.$$

d_{CDV} was set to -206.4‰ due to the isotopic ratio of the CDV added into the model. Using this method, the maximum contribution of the CDV to the atmospheric humidity could be estimated.

Besides the second method, the CDV fraction was also calculated based on isotopic observations. The approach was similar to that of a previous method, albeit with some modifications. Due to the lack of d_{nat} (isotopic ratio of atmospheric moisture in the absence of CDV), a different approach was employed. First, 10% of the observed data with the highest d-excess values were selected and assumed to have no CDV impact. These data points represented the natural background without CDV influence. Subsequently, a regression line was established in the $^{2}H/^{18}O$ plot representing the natural background line. More details regarding this method can be found in the Appendix. It is important to note that this method assumes that all d-excess decreases can be attributed to the CDV impact, which may not be entirely realistic. Therefore, the estimation obtained using this method serves as a reference for comparison with the simulation results.

3 Results

3.1 Time series

Figure 1 presents the time series and diurnal variations of various parameters, including the planetary boundary layer height, 2-m air temperature, 2-m specific humidity, and 2-m vapor d-excess in both SLC and Beijing, and shows that the CDV addition had a negligible effect on the simulated air temperature. In SLC, the monthly mean temperature decreased slightly from 269.75 to 269.49 K, whereas in Beijing, the temperature increased marginally from 266.96 to 266.99 K. Conversely, the simulation indicated a more noticeable increase in specific humidity after adding CDV, particularly in Beijing with an increase of 0.1230 g/kg compared to the smaller increase of 0.0160 g/kg at SLC.

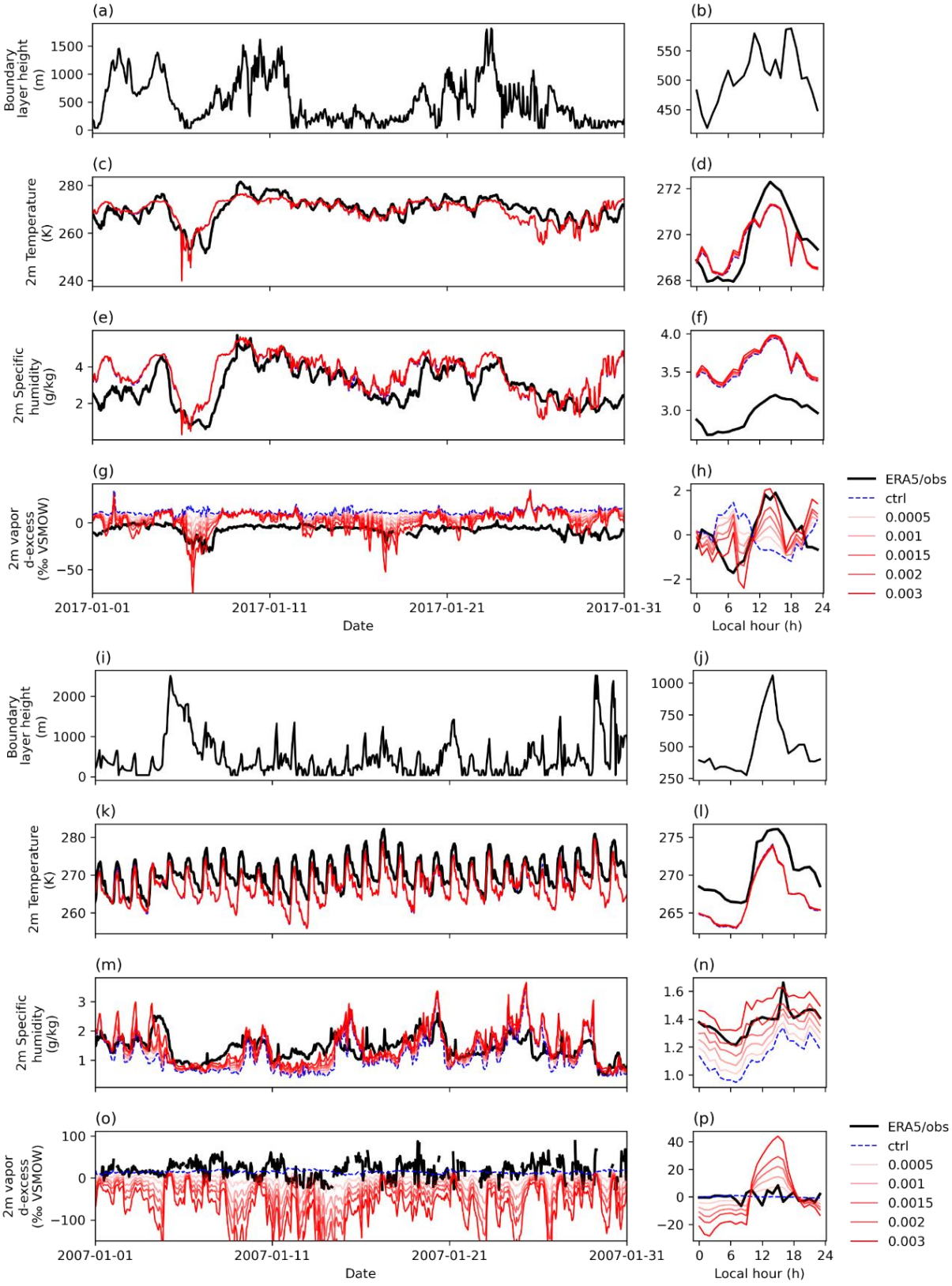

Figure 1. Time series and diurnal variation of boundary layer height (m), 2m air temperature (K), 2m specific humidity (g/kg), and 2m vapor d-excess (‰) in SLC (a-h) and Beijing (i-p). The black lines are ERA5 reanalysis data or in-situ observation, the blue dashed lines are the simulation without CDV, and the red lines are the simulation with CDV.

237

238 **Table 2** Correlation coefficient, RMSE and Residual standard deviation of observed 2m vapor d-excess and each experiment

Site	Experiment	Correlation coefficient	RMSE	Residual standard deviation
Salt Lake City	Ctrl	-0.2207	20.4743	6.9503
	0.0005	0.0796	18.2682	6.3959
	0.0010	0.2690	16.3777	6.3583
	0.0015	0.3537	14.8922	6.9751
	0.0020	0.4058	13.7362	7.9219
	0.0030	0.4559	12.9047	10.6402
Beijing	Ctrl	-0.0569	21.0852	20.5319
	0.0005	0.0380	30.0539	22.2266
	0.0010	0.0502	45.2486	27.8657
	0.0015	0.0536	62.4340	35.7632
	0.0020	0.0577	80.2537	44.5966
	0.0030	0.0613	116.8704	63.7893

239

240 **Table 2** lists the correlation coefficient, root mean square error (RMSE), and residual
241 standard deviations for the different experiments. In SLC, all four experiments exhibited
242 d-excess overestimations in most periods compared to the observed data. The observed
243 monthly mean d-excess value was -7.52‰, i.e., significantly lower than the simulated values
244 (from 11.75‰ for the control to -0.53‰ for 0.003 $g/m^2 \cdot s$). The CDV impact was more
245 pronounced when the planetary boundary layer height was lower, indicating a more stable
246 atmosphere. With an increase in the CDV emission rate, the correlation coefficient increased
247 owing to the increasingly significant variation. However, the residual standard deviation
248 suggested that a higher emission rate could result in a variation range higher than that
249 observed, thereby worsening the simulation performance. Overall, the 0.0015 $g/m^2 \cdot s$
250 emission rate had the best simulating result in SLC, and was therefore used in the subsequent
251 analysis part. At 9:00 on January 6, 2017, the d-excess difference between the control and
252 CDV experiment peaked at approximately 33‰. This finding suggests that the CDV impact
253 was greater under conditions of low boundary layer height, low temperature, and low
254 humidity. The d-excess reduction resulted in a better fit with the observations, as evidenced
255 by the correlation coefficient increasing from -0.22 to 0.35.
256 In Beijing, prior to the CDV addition, the d-excess values exhibited a relatively stable
257 trend compared to that of the observed data. However, the CDV introduction led to a
258 significant fluctuation increase. Interestingly, the observed monthly mean vapor (19.19‰)
259 was higher than that of the control simulation (14.42‰), thereby contradicting the CDV
260 impact. Following the modification with CDV, the monthly mean d-excess sharply decreased

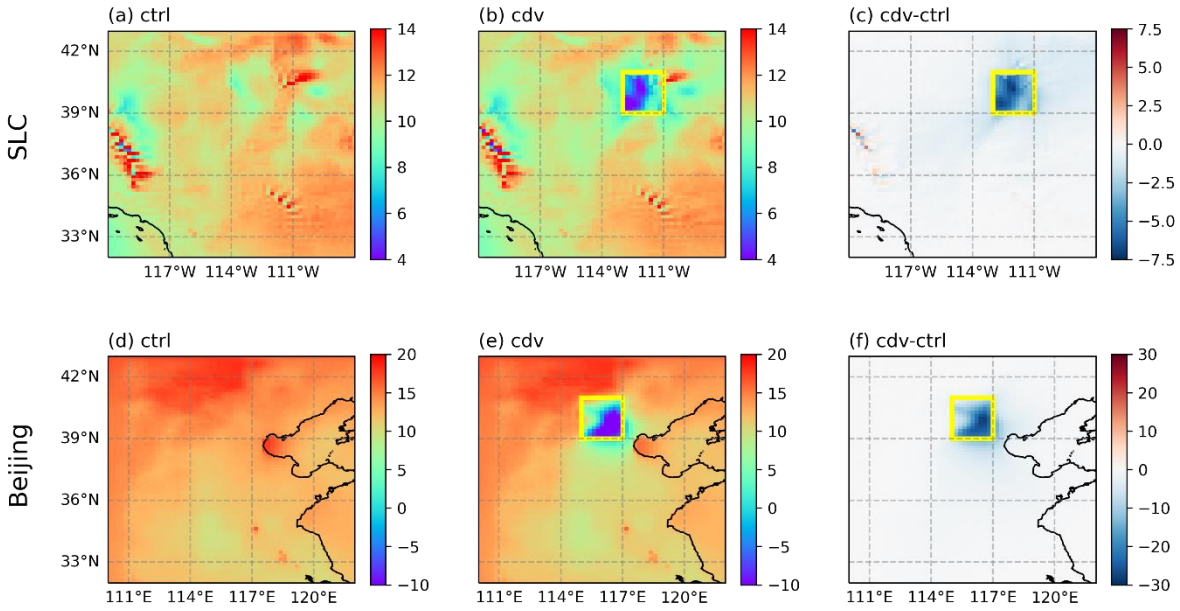

Figure 2. Monthly mean 2m vapor d-excess (‰) and the differences between modified experiments and control one in SLC (a-c) and Beijing (d-f). The yellow boxes show the domain that CDV was added.

to -16.00‰. The CDV inclusion slightly improved the correlation coefficient between the simulation and observations. However, the highest correlation coefficient was only 0.0613 for the case with an emission rate of 0.003 g/m^2·s, thereby still lacking significance. Furthermore, the RMSE noticeably increased after the CDV addition, owing to the lower d-excess values; and the residual standard deviation increased significantly when the emission rate was above 0.001 g/m^2·s, indicating that the fluctuation of simulation became higher than observation. Therefore, the CDV emission rate of 0.001 g/m^2·s was selected to represent the best simulation in Beijing and was therefore used in the subsequent analysis part.

The diurnal variation of Δd-excess along with the mean value is shown in **Figure 1(h)** and **1(p)**. The diurnal SLC variation range was lower than that in Beijing, making the variation in the simulations without CDV more pronounced. However, these results without CDV impact displayed an opposite trend compared to the observations. The CDV inclusion in the simulations partially reduced this opposite variation by decreasing the d-excess during nighttime and increasing it during daytime. This effect was more prominent in Beijing. The diurnal variation of the observed data was much higher than that of the simulation without CDV. The CDV addition improved dramatically the variation, bringing it closer to the range of the observations. This improvement was attributed to the difference in humidity between day and night. With lower humidity during nighttime, the proportion of the fixed CDV amount would be higher, resulting in lower d-excess values. Overall, these findings indicated that the addition of CDV could significantly enhance the simulation of the diurnal variation of vapor d-excess.

3.2 Spatial distribution

Figure 2 displays the monthly average distribution of 2-m vapor d-excess in the four experiments, as well as the differences between the three modified experiments and the control experiment. The results indicated that the CDV inclusion led to a significant vapor d-excess reduction within the urban domains. Additionally, owing to moisture diffusion, a

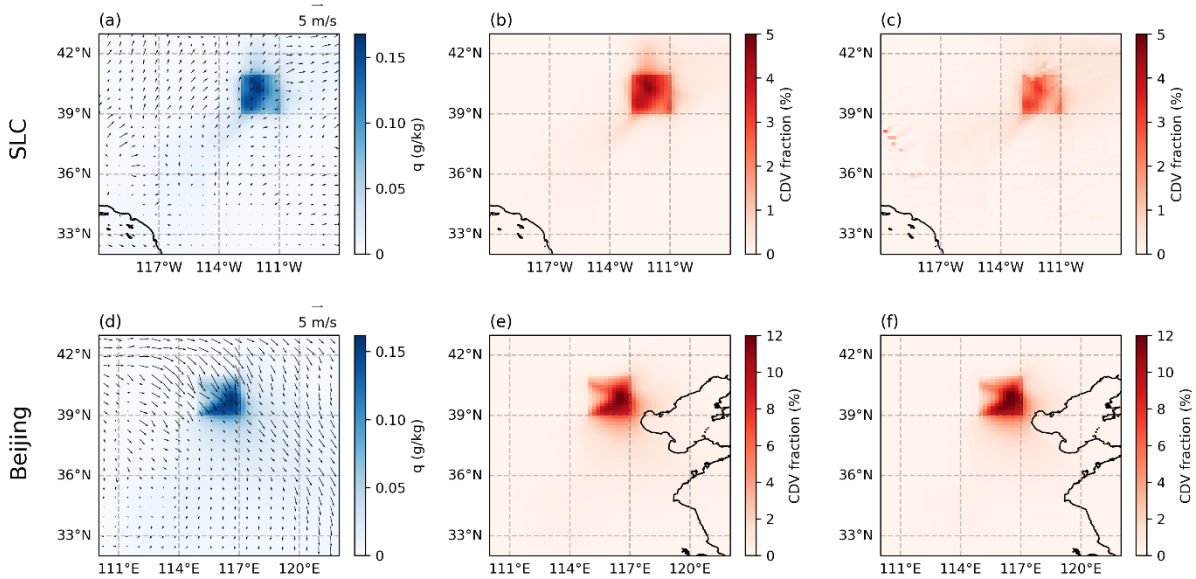

Figure 3. Monthly mean specific humidity (g/kg) caused by the CDV emission and CDV fraction (%) in the total 2m moisture in SLC (a-c) and Beijing (d-f). Monthly mean 10m wind fields are also shown in (a) and (d).

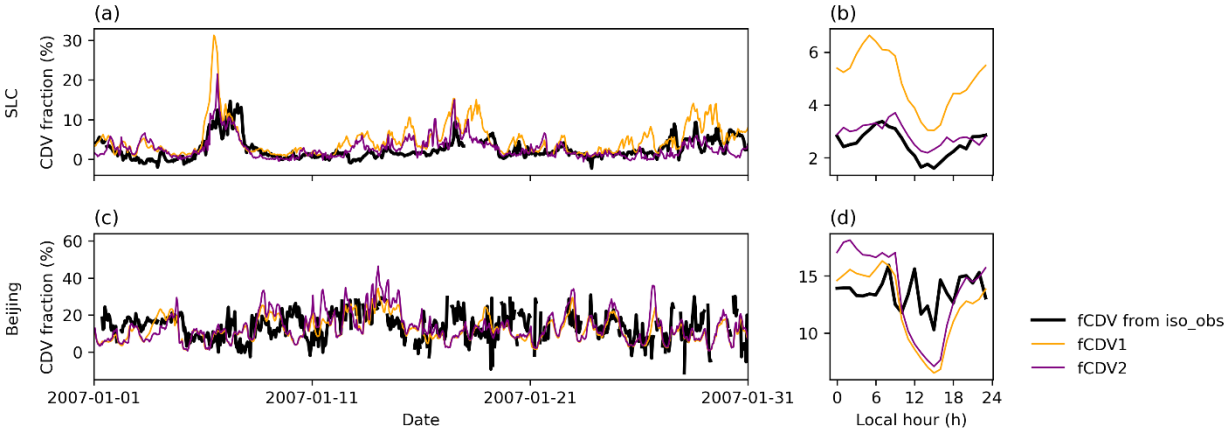

Figure 4. Time series and diurnal variation of CDV fraction (%) in SLC (a,b) and Beijing (c,d). Black lines are calculated from in-situ observation. Orange lines are calculated from the moisture tracer method. Purple lines are calculated from the mixing equation and simulated d-excess.

slight d-excess decrease was observed in the surrounding areas, whereas the other domains remained unaffected. When the same CDV emission rate was applied, the d-excess decrease in SLC was approximately 5‰, which was notably lower than the decrease observed in Beijing. This difference could be attributed to the higher specific humidity in SLC during January, resulting in a lower CDV proportion in the total moisture content, and consequently, a weaker impact on vapor d-excess.

3.3 CDV fraction

As shown in **Figure 3(a)** and **3(d)**, there was no significant difference in the monthly mean specific humidity caused by CDV between SLC and Beijing. However, owing to the higher specific humidity, the CDV fraction was significantly lower in SLC. The monthly 10-m wind field explained the direction of the CDV diffusion. The higher wind speed in Beijing could

also cause a greater kinetic fractionation effect on the land surface in this domain.

The time series and diurnal variation of the CDV fraction are presented in **Figure 4**. In SLC, the monthly mean CDV fraction calculated using the moisture tracer method (fCDV1) was 4.9%, i.e., 2% higher than that obtained using the mixing equation method (fCDV2). In Beijing, fCDV1 was estimated to be approximately 12.3%, i.e., lower than fCDV2 (13.8%).

Table 3 provides the correlation coefficients and RMSEs between these CDV fraction values and the estimates derived from the observed data. SLC exhibited significantly higher correlation coefficients and lower RMSEs than those of Beijing, indicating that impact of a fixed emission rate of CDV can be used to explain the variation of d-excess in the observed data of SLC, but fails to simulate the similar pattern in the observation of Beijing.

Table 3 Correlation coefficient and RMSE of the fraction of CDV from observation and each method

Site	Method	Correlation coefficient	RMSE
SLC	fCDV1	0.6524	3.8030
	fCDV2	0.5329	2.5706
Beijing	fCDV1	0.1505	9.5450
	fCDV2	0.0683	11.4817

4 Discussion

4.1 Relationship between humidity and vapor d-excess

The relationship between humidity and vapor d-excess is shown in **Figure 5**. The control experiment in the original IsoRSM simulation revealed no significant correlation between specific humidity and vapor d-excess. However, the CDV addition had a stronger impact on the vapor d-excess reduction when humidity was lower. This effect aligns with the observed results in SLC, suggesting that the CDV inclusion can improve the relationship between humidity and vapor d-excess at this location. This relationship can be explained by the CDV fraction in the total atmospheric moisture, as demonstrated by the earlier diurnal variation analysis. With a fixed CDV amount, lower humidity from natural sources would result in a higher CDV impact, and this change caused by CDV would be more pronounced when the atmosphere was relatively stable. However, the observations from Beijing showed a different correlation, i.e., a low specific humidity corresponded to higher observed d-excess values. This phenomenon indicated the presence of other moisture sources with higher d-excess values contributing to the distinctive correlation between humidity and vapor d-excess in SLC and Beijing. Overall, these findings suggest that the relationship between humidity and vapor d-excess is influenced by the presence of CDV and other moisture sources, highlighting the complexity of the isotopic composition in different environments.

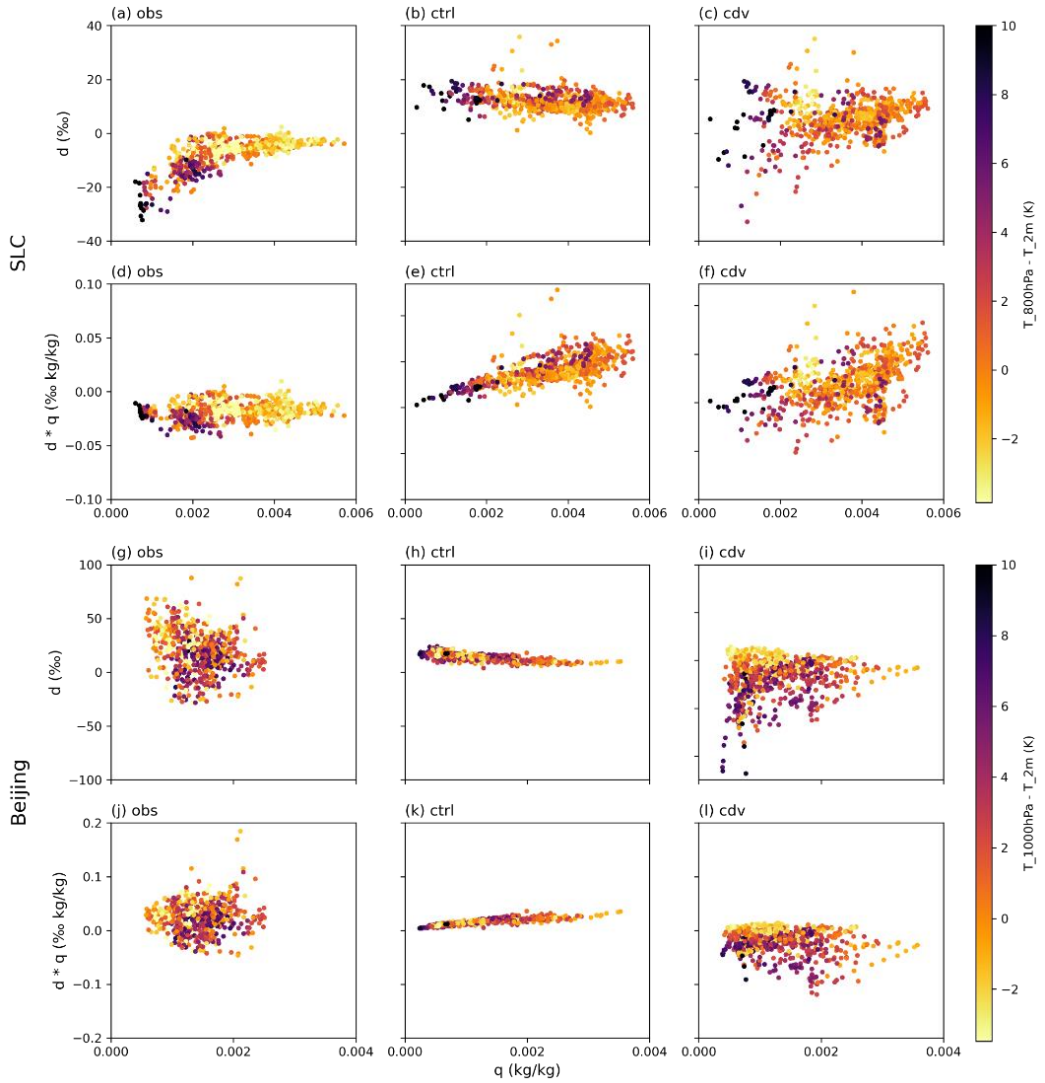

Figure 5. Relationship between 2m specific humidity (q, kg/kg) and 2m vapor d-excess (d, ‰), and the relationship between q and d*q (‰·kg/kg) in SLC (a-f) and Beijing(g-i). The color of the dots shows the temperature differences between 2m and 800hPa for SLC and 1000hPa for Beijing, which can be regarded as an indicator for describing atmospheric stability.

To figure out the source of high d-excess moisture in Beijing, an individual experiment which considered the kinetic fractionation effect in the evaporating process on the land surface was made. Due to this experiment was not particularly relevant to the topic of this study, the results were not displayed in this article. Based on the experiment, the simulation in SLC showed a d-excess reduction when humidity was high, whereas in Beijing, the simulation indicated that d-excess was increased when humidity was low. Therefore, it is possible that the kinetic fractionation effect on the land surface is one of the factors contributing to the higher d-excess in Beijing (Lee et al., 2009; Kei Yoshimura et al., 2006). The specific mechanisms and processes involved would require further investigation to better understand the observed relationship between humidity and d-excess in Beijing and the influence of the kinetic fractionation effect.

4.2 Humidity increase caused by CDV and the CDV fraction

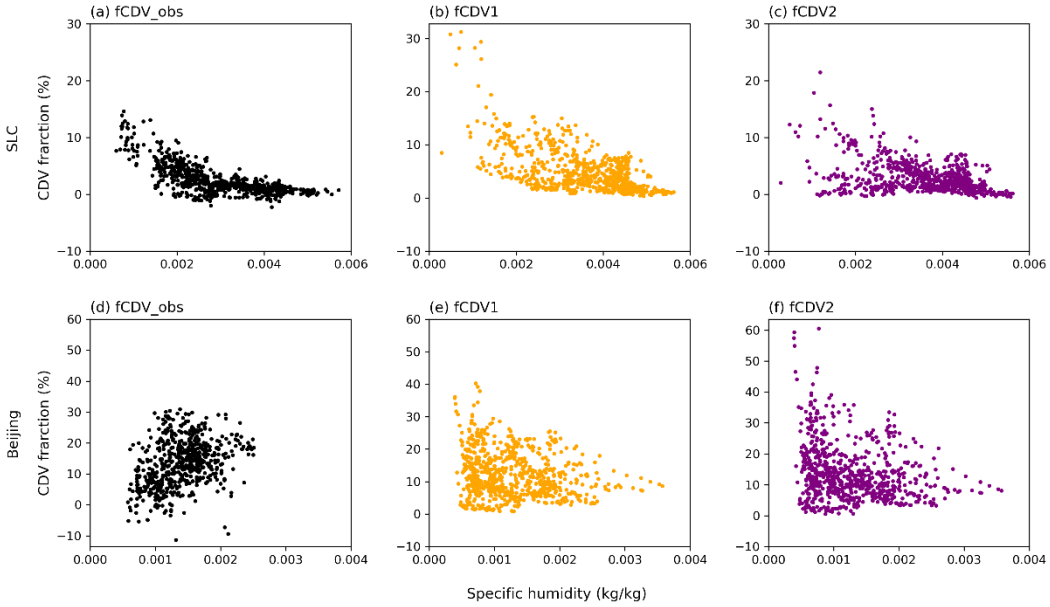

Figure 6. Relationship between specific humidity (kg/kg) and CDV fraction (%) in SLC (a-d) and Beijing (e-h). The color of dots indicates the same meaning in Figure5.

As shown in **Figure 1(e)** and **1(m)**, the specific humidity increase caused by the CDV in SLC was not as significant as that in Beijing. Using the moisture tracer method, moisture at these two sites could be divided into local evaporation and remote transportation sources. **Figure S2** shows that in SLC, the CDV addition decreased the moisture transported from remote areas. However, this decrease was not observed in the Beijing simulation. Therefore, the specific humidity in SLC did not show an obvious increase, which may have influenced the calculation of the CDV fraction using the moisture tracer method.

The findings in the CDV fraction time series were consistent with the relationship between the CDV fraction and humidity, as depicted in **Figure 6**. All results from the observations and simulations demonstrated a negative correlation between specific humidity and the CDV fraction, except for the observational data in Beijing. The discrepancy between the CDV fraction values obtained from observations and simulations indicated that the vapor d-excess decrease in SLC could be explained by CDV emissions, whereas the CDV impact alone could not fully account for the d-excess variation in Beijing in winter.

To determine the reason for the higher estimated value of the CDV fraction in the moisture tracer method than that in the mixing equation method in SLC, the mixing process of CDV and natural source vapor was theoretically calculated. As the moisture tracer function could directly obtain the specific humidity caused by CDV (here, $q_{CDV}{}'$), it was possible to calculate the $(q*d)_{mix}{}'$ using the two end-member mixing equations:

$$(q*d)'_{mix} = q_{nat}*d_{nat} + q'_{CDV}*d_{CDV}.$$

The $(q*d)_{mix}{}'$ indicates the q*d mixed by the moisture of natural sources and CDV with the amount obtained from the moisture tracer method. Then the $d_{mix}{}'$ can be calculated, as follows:

$$d'_{mix} = \frac{(q*d)'_{mix}}{q_{nat} + q'_{CDV}}.$$

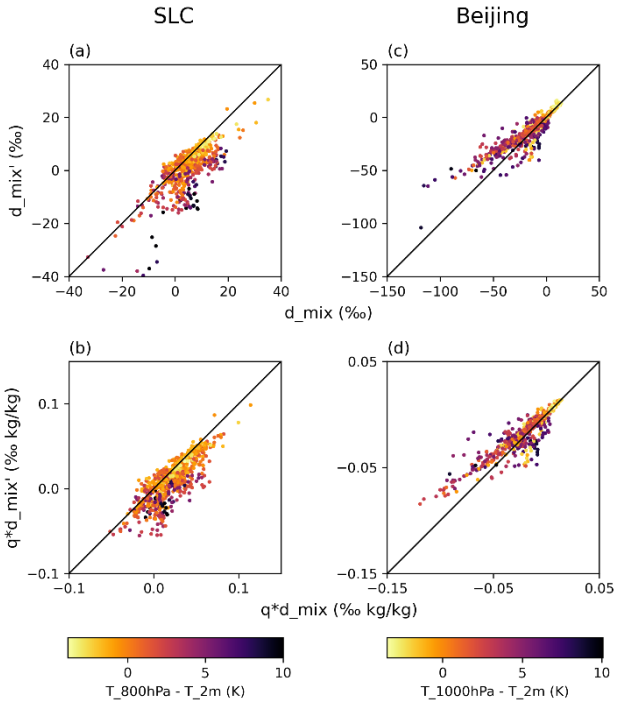

Figure 7. Comparison between d_mix and d_mix', q*d_mix and q*d_mix' in SLC (a,b) and Beijing (c,d). The colorbar showed the same information as Figure 5.

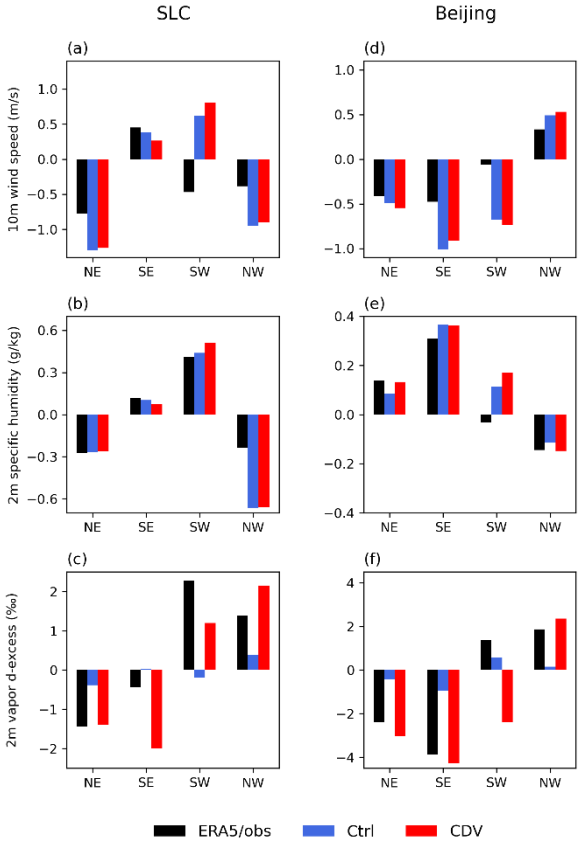

Figure 8. Monthly mean 10m wind speed (m/s), 2m specific humidity (g/kg) and vapor d-excess (‰) anomalies in different wind directions in SLC (a-c) and Beijing (d-f).

Figure 7 shows a comparison of d_{mix} with $(q * d)_{mix}$ from the model simulation and the calculation. The results indicate that the CDV impact on vapor d-excess was slightly underestimated in SLC and overestimated in Beijing, considering the CDV amount in the simulation; and the bias between d_{mix} and d'_{mix} was higher when the boundary condition was more stable in SLC. This phenomenon might have been caused by the different atmospheric conditions at these two sites.

4.3 d-excess difference among wind directions

Moisture transportation is mainly controlled by wind direction and speed. Therefore, the vapor d-excess difference among the wind directions could reflect different moisture sources. **Figure 8** shows the monthly anomalies of wind speed, specific humidity, and vapor d-excess for different wind directions. In the case of SLC, the observational data revealed that the easterly wind direction involved vapor d-excess that was about 2‰ lower compared to that of the westerly wind directions. This finding indicated that moisture originating from the east had a greater influence on CDV. The simulations with CDV emissions also reproduced this difference among wind directions, where lower vapor d-excess values were predominantly observed with easterly winds. This consistency between the observed and simulated characteristics further supported the notion that CDV emissions play a significant role in the vapor d-excess variation in SLC.

The observational data in Beijing revealed a higher vapor d-excess value when the wind was northwesterly and a relatively lower d-excess value when the wind was southerly. Referring to previous research, the northwest of Beijing, which corresponds to the inland area of North China, had a higher vapor d-excess when the isotopic fractionation effect on the land surface was considered in the model. This suggests that the higher d-excess with the northwesterly wind could be transported from the inland area. **Table 4** shows the correlation coefficients between observed and simulated vapor d-excess for different wind directions, and the linear regression line of the observation and simulation can be seen in **Figure S3**. When the wind was southerly, the correlation coefficient showed a significant improvement after adding CDV, thereby indicating that during these periods, the CDV impact was likely the dominating factor of the vapor d-excess. In contrast, the correlation coefficient decreased when the wind was northeasterly, indicating that the CDV inclusion did not improve the d-excess simulation in this moisture source.

Table 4 Correlation coefficient of vapor d-excess in observation and simulation with different wind directions

Site	Wind direction	Ctrl	CDV
SLC	NE	-0.2690	-0.0942
	SE	-0.3467	0.4791
	SW	-0.1710	0.0717
	NW	-0.1806	-0.0641
Beijing	NE	-0.0102	-0.2164
	SE	-0.2730	0.2919
	SW	-0.1048	0.2770
	NW	-0.0377	0.0284

5 Summary and Conclusions

In this study, the isotope-enabled regional spectral model (IsoRSM) was used to simulate the combustion-derived vapor (CDV) emissions in urban areas and determine whether anthropogenic emissions influence the isotopic ratio of water in the urban atmosphere. Two separate one-month experiments were conducted: one in Salt Lake City (SLC) in January 2017 and another in Beijing in January 2007. By adding an extra amount of vapor with a fixed isotopic ratio to the 2°×2° domains during the evaporation process, the CDV emissions in the urban areas could be roughly simulated.

The simulation results demonstrated that the introduction of CDV emissions significantly reduced the d-excess of water vapor, particularly when the boundary layer was stable. The d-excess decrease in Beijing was more pronounced than that in SLC because of higher humidity from natural sources in SLC. The simulation with CDV emissions showed better agreement with the time series of the in-situ observations in SLC than the original model. However, in Beijing, the observed vapor d-excess exhibited stronger fluctuations but was occasionally higher than the simulated values, contrary to the expected CDV impact. Despite this discrepancy, the CDV addition improved the simulation by enhancing the diurnal variation of d-excess, resulting in a pattern that closely resembled the observations.

The inclusion of a fixed CDV amount in the simulations led to a positive correlation between vapor d-excess and specific humidity, which was consistent with the observations in SLC and inconsistent with the observations in Beijing. The d-excess underestimation at lower humidity levels in Beijing might be caused by the kinetic fractionation effect during the evaporation process on the land surface in the inland areas. The moisture with higher d-excess could be transported by the strong winter monsoon in Beijing. This phenomenon indicated that the CDV should not be the only controlling factor of the variation of vapor d-excess in some domains.

The moisture tracer method and mixing equation were both employed to estimate the CDV fraction in the total 2-m moisture. The moisture tracer method yielded a monthly mean CDV fraction (fCDV1) of 3.3% in SLC and 12.3% in Beijing. The CDV fraction derived from the d-excess value and mixing equation (fCDV2) exhibited a similar trend to that of fCDV1, albeit slightly underestimated in SLC and overestimated in Beijing. Both fCDV1 and fCDV2 were negatively correlated with specific humidity, in contrast to the CDV fraction derived from observations in Beijing. These findings suggest that a fixed amount of CDV emissions alone cannot fully account for the vapor d-excess variations observed in Beijing.

Dividing the observed and simulated data based on different wind directions allowed the analysis of moisture transportation effects. The vapor d-excess diversity was enhanced with the CDV inclusion and was more similar to those of the observations at both sites. In Beijing, higher d-excess values were observed under northwesterly winds, suggesting the possible transport from inland areas with a stronger kinetic fractionation effect. Conversely, weaker easterly winds resulted in lower d-excess values, indicating a higher impact of CDV with these sources of moisture.

In conclusion, although there were some biases caused by the underestimation of d-excess variation from natural sources, CDV could be one of the controlling factors of atmospheric vapor d-excess in some urban areas such as SLC. For these regions, the inclusion of CDV in the model would significantly improve the bias, temporal and diurnal variations, and enhance the correlation between vapor d-excess and local humidity. Therefore, it is of great potential to use atmospheric models to simulate anthropogenic vapor emissions.

Several aspects of this study can be improved. One important improvement would be the development of a CDV emission map based on the amount of emitted CO_2. This approach should provide a more realistic representation of the CDV emission sources in urban areas. By incorporating such an emission map into the model simulation, the results should become more reliable and accurate, leading to a better understanding of the CDV influence on the isotopic ratio of water vapor in the urban atmosphere. This improvement should enhance the credibility and applicability of the research findings.

Data Available Statement

The hourly observed vapor isotope data in Salt Lake City are available at https://osf.io/k47ft (Fiorella et al., 2019). And the hourly observed vapor isotope data in Beijing are available at https://vapor-isotope.yale.edu/sites-and-dataset/asia/cn-beijing (Wen et al., 2010). ERA5 reanalysis data are available at https://cds.climate.copernicus.eu/cdsapp#!/search?type=dataset%26text=ERA5 (Hersbach et

al., 2020). The data analysis and figure construction in this study were performed using the open-source Python language v3.11.4 (https://www.python.org/) and the Grid Analysis and Display System v2 software (http://cola.gmu.edu/grads/).

Acknowledgment

This work was supported by JST SPRING (JPMJSP2108), the Environment Research and Technology Development Fund S-20 of the Environmental Restoration and Conservation Agency of Japan (JPMEERF21S12020), Earth Observation Research Center, Japan Aerospace Exploration Agency (JX-PSPC-533980), the Japan Society for the Promotion of Science via Grants-in-Aid (21H05002, 22H04938), JST-Mirai Program (JPMJMI21I6), JST-Moonshot Program (JPMJMS2282-08), JST-eASIA Joint Research Program (JPMJSC22E4), MEXT program for the advanced studies of climate change projection SENTAN (JPMXD0722680395, JPMXD1420318865), Cross-ministerial Strategic Innovation Promotion Programs (SIP) Enhancement of National Resilience against Natural Disasters (Funding agency: NIED).

References

Bergeron, O., & Strachan, I. B. (2012). Wintertime radiation and energy budget along an urbanization gradient in Montreal, Canada. *International Journal of Climatology*, *32*(1), 137–152. https://doi.org/10.1002/joc.2246

Blossey, P. N., Kuang, Z., & Romps, D. M. (2010). Isotopic composition of water in the tropical tropopause layer in cloud-resolving simulations of an idealized tropical circulation. *Journal of Geophysical Research Atmospheres*, *115*(24). https://doi.org/10.1029/2010JD014554

Carlton, A. G., & Turpin, B. J. (2013). Particle partitioning potential of organic compounds is highest in the Eastern US and driven by anthropogenic water. *Atmospheric Chemistry and Physics*, *13*(20), 10203–10214. https://doi.org/10.5194/acp-13-10203-2013

Chang, E. C., & Yoshimura, K. (2015). A semi-Lagrangian advection scheme for radioactive tracers in the NCEP Regional Spectral Model (RSM). *Geoscientific Model Development*, *8*(10), 3247–3255. https://doi.org/10.5194/gmd-8-3247-2015

Dansgaard, W. (1964). Stable isotopes in precipitation. *Tellus*, *16*(4), 436–468. https://doi.org/10.1111/j.2153-3490.1964.tb00181.x

Fiorella, R. P., Poulsen, C. J., Pillco Zolá, R. S., Barnes, J. B., Tabor, C. R., & Ehlers, T. A. (2015). Spatiotemporal variability of modern precipitation δ 18 O in the central Andes and implications for paleoclimate and paleoaltimetry estimates. *Journal of Geophysical Research*, *120*(10), 4630–4656. https://doi.org/10.1002/2014JD022893

Fiorella, R. P., Bares, R., Lin, J. C., Ehleringer, J. R., & Bowen, G. J. (2018). Detection and variability of combustion-derived vapor in an urban basin. *Atmospheric Chemistry and Physics*, *18*(12), 8529–8547. https://doi.org/10.5194/acp-18-8529-2018

Fiorella, R. P., Bares, R., Lin, J. C., & Bowen, G. J. (2019). Wintertime decoupling of urban valley and rural ridge hydrological processes revealed through stable water isotopes. *Atmospheric Environment*, *213*, 337–348. https://doi.org/10.1016/j.atmosenv.2019.06.022

Gorski, G., Strong, C., Good, S. P., Bares, R., Ehleringer, J. R., & Bowen, G. J. (2015). Vapor hydrogen and oxygen isotopes reflect water of combustion in the urban atmosphere. *Proceedings of the National Academy of Sciences of the United States of America*, *112*(11), 3247–3252.

https://doi.org/10.1073/pnas.1424728112

Hersbach, H., Bell, B., Berrisford, P., Hirahara, S., Horányi, A., Muñoz-Sabater, J., et al. (2020). The ERA5 global reanalysis. *Quarterly Journal of the Royal Meteorological Society*, *146*(730), 1999–2049. https://doi.org/10.1002/qj.3803

Hirano, T., Sugawara, H., Murayama, S., & Kondo, H. (2015). Diurnal variation of CO2 flux in an urban area of Tokyo. *Scientific Online Letters on the Atmosphere*, *11*, 100–103. https://doi.org/10.2151/sola.2015-024

Huntington, T. G. (2006). Evidence for intensification of the global water cycle: Review and synthesis. *Journal of Hydrology*, *319*(1–4), 83–95. https://doi.org/10.1016/j.jhydrol.2005.07.003

Kanamaru, H., & Kanamitsu, M. (2007). Scale-selective bias correction in a downscaling of global analysis using a regional model. *Monthly Weather Review*, *135*(2), 334–350. https://doi.org/10.1175/MWR3294.1

Kanamitsu, M., Kanamaru, H., Cui, Y., Juang, H., 2005. Parallel Implementation of the Regional Spectral Atmospheric Model. CEC Tech. Rep. CEC-500-2005-014, California Energy Commission, 19 pp., https://www.coaps.fsu.edu/prediction/G-RSM/cec_report1.pdf

Kanamitsu, M., Yoshimura, K., Yhang, Y. Bin, & Hong, S. Y. (2010). Errors of interannual variability and trend in dynamical downscaling of reanalysis. *Journal of Geophysical Research Atmospheres*, *115*(17). https://doi.org/10.1029/2009JD013511

Lee, X., Griffis, T. J., Baker, J. M., Billmark, K. A., Kim, K., & Welp, L. R. (2009). Canopy-scale kinetic fractionation of atmospheric carbon dioxide and water vapor isotopes. *Global Biogeochemical Cycles*, *23*(1). https://doi.org/10.1029/2008GB003331

Li, Xiaoyang, Kawamura, R., Sugimoto, A., & Yoshimura, K. (2021). Estimation of water origins within an explosive cyclone over the Sea of Japan using an isotopic regional spectral model. *Journal of Hydrometeorology*. https://doi.org/10.1175/jhm-d-21-0027.1

Li, Xin, Fan, W., Wang, L., Luo, M., Yao, R., Wang, S., & Wang, L. (2021). Effect of urban expansion on atmospheric humidity in Beijing-Tianjin-Hebei urban agglomeration. *Science of the Total Environment*, *759*. https://doi.org/10.1016/j.scitotenv.2020.144305

Liu, S., Pang, H., Zhang, N., Xing, M., Wu, S., & Hou, S. (2022). Temporal variations of the contribution of combustion-derived water vapor to urban humidity during winter in Xi'an, China. *Science of the Total Environment*, *830*. https://doi.org/10.1016/j.scitotenv.2022.154711

Loaiciga A', H. A., Valdes, J. B., Vogel, R., Garvey, J., & Schwarz, H. (1996). *Global warming and the hydrologic cycle*. *Journal of Hydrology ELSEVIER Journal of Hydrology* (Vol. 174).

McCarthy, M. P., Best, M. J., & Betts, R. A. (2010). Climate change in cities due to global warming and urban effects. *Geophysical Research Letters*, *37*(9). https://doi.org/10.1029/2010GL042845

Mckain, K., Wofsy, S. C., Nehrkorn, T., Eluszkiewicz, J., Ehleringer, J. R., & Stephens, B. B. (2012). Assessment of ground-based atmospheric observations for verification of greenhouse gas emissions from an urban region. *ATMOSPHERIC, AND PLANETARY SCIENCES*, *109*(22), 8423–8428. https://doi.org/10.1073/pnas.1116645109/-/DCSupplemental

Merlivat, L., & Jouzel, J. (1979). Global climatic interpretation of the deuterium-oxygen 16 relationship for precipitation. *Journal of Geophysical Research*, *84*(C8), 5029–5033. https://doi.org/10.1029/JC084iC08p05029

Moriwaki, R., Kanda, M., Senoo, H., Hagishima, A., & Kinouchi, T. (2008). Anthropogenic water vapor emissions in Tokyo. *Water Resources Research*, *44*(11). https://doi.org/10.1029/2007WR006624

Pisso, I., Patra, P., Takigawa, M., Machida, T., Matsueda, H., & Sawa, Y. (2019). Assessing Lagrangian

inverse modelling of urban anthropogenic CO2 fluxes using in situ aircraft and ground-based measurements in the Tokyo area. *Carbon Balance and Management*, *14*(1). https://doi.org/10.1186/s13021-019-0118-8

Rosenfeld, D., Lohmann, U., Raga, G. B., O'dowd, C. D., Kulmala, M., Fuzzi, S., et al. (2008). Flood or Drought: How Do Aerosols Affect Precipitation? *Science*, *321*(5894), 1309–1313. https://doi.org/DOI: 10.1126/science.1160606

Sailor, D. J. (2011). A review of methods for estimating anthropogenic heat and moisture emissions in the urban environment. *International Journal of Climatology*, *31*(2), 189–199. https://doi.org/10.1002/joc.2106

Salmon, O. E., Shepson, P. B., Ren, X., Marquardt Collow, A. B., Miller, M. A., Carlton, A. G., et al. (2017). Urban emissions of water vapor in winter. *Journal of Geophysical Research: Atmospheres*, *122*(17), 9467–9484. https://doi.org/10.1002/2016JD026074

Tie, X., Huang, R. J., Cao, J., Zhang, Q., Cheng, Y., Su, H., et al. (2017). Severe Pollution in China Amplified by Atmospheric Moisture. *Scientific Reports*, *7*(1). https://doi.org/10.1038/s41598-017-15909-1

Ueyama, M., Taguchi, A., & Takano, T. (2021). Water vapor emissions from urban landscapes in Sakai, Japan. *Journal of Hydrology*, *598*. https://doi.org/10.1016/j.jhydrol.2021.126384

Wei, Z., Lee, X., Aemisegger, F., Benetti, M., Berkelhammer, M., Casado, M., et al. (2019). A global database of water vapor isotopes measured with high temporal resolution infrared laser spectroscopy. *Scientific Data*, *6*. https://doi.org/10.1038/sdata.2018.302

Wen, X. F., Zhang, S. C., Sun, X. M., Yu, G. R., & Lee, X. (2010). Water vapor and precipitation isotope ratios in Beijing, China. *Journal of Geophysical Research Atmospheres*, *115*(1). https://doi.org/10.1029/2009JD012408

Wu, J., Bei, N., Liu, W., Xing, M., Liu, S., Song, T., et al. (2022). Why is the air humid during wintertime heavy haze days in Beijing? *Science of the Total Environment*, *853*. https://doi.org/10.1016/j.scitotenv.2022.158597

Xing, M., Liu, W., Li, X., Zhou, W., Wang, Q., Tian, J., et al. (2020). Vapor isotopic evidence for the worsening of winter air quality by anthropogenic combustion-derived water. *Proceedings of the National Academy of Sciences of the United States of America*, *117*(52), 33005–33010. https://doi.org/10.1073/pnas.1922840117/-/DCSupplemental

Yoshimura, Kei, & Kanamitsu, M. (2008). Dynamical global downscaling of global reanalysis. *Monthly Weather Review*, *136*(8), 2983–2998. https://doi.org/10.1175/2008MWR2281.1

Yoshimura, Kei, Miyazaki, S., Kanae, S., & Oki, T. (2006). Iso-MATSIRO, a land surface model that incorporates stable water isotopes. *Global and Planetary Change*, *51*(1-2 SPEC. ISS.), 90–107. https://doi.org/10.1016/j.gloplacha.2005.12.007

Yoshimura, Kei, Kanamitsu, M., & Dettinger, M. (2010). Regional downscaling for stable water isotopes: A case study of an atmospheric river event. *Journal of Geophysical Research Atmospheres*, *115*(18). https://doi.org/10.1029/2010JD014032

Yoshimura, Kie, & Kanamitsu, M. (2009). Specification of external forcing for regional model integrations. *Monthly Weather Review*, *137*(4), 1409–1421. https://doi.org/10.1175/2008MWR2654.1